Author Manuscript

Author Manuscript

Author Manuscript

Author Manuscript

HHS Public Access

Author manuscript

Biomaterials. Author manuscript; available in PMC 2016 November 01.

Published in final edited form as:

Biomaterials. 2015 November ; 69: 65–75. doi:10.1016/j.biomaterials.2015.08.011.

MRI Evaluation of Injectable Hyaluronic Acid-Based Hydrogel Therapy to Limit Ventricular Remodeling after Myocardial Infarction

Shauna M. Dorsey[a], **Jeremy R. McGarvey**[b], **Hua Wang**[c], **Amir Nikou**[c], **Leron Arama**[a], **Kevin J. Koomalsingh**[b], **Norihiro Kondo**[b], **Joseph H. Gorman III**[b], **James J. Pilla**[a,e], **Robert C. Gorman**[b], **Jonathan F. Wenk**[c,d], and **Jason A. Burdick**[a,*]

[a]Department of Bioengineering, University of Pennsylvania, Philadelphia, PA 19104, USA

[b]Gorman Cardiovascular Research Group, Department of Surgery, University of Pennsylvania, Philadelphia, PA 19104, USA

[c]Department of Mechanical Engineering, University of Kentucky, Lexington, KY 40506, USA

[d]Department of Surgery, University of Kentucky, Lexington, KY 40506, USA

[e]Department of Radiology, University of Pennsylvania, Philadelphia, PA 19104, USA

Abstract

Injectable biomaterials are an attractive therapy to attenuate left ventricular (LV) remodeling after myocardial infarction (MI). Although studies have shown that injectable hydrogels improve cardiac structure and function *in vivo*, temporal changes in infarct material properties after treatment have not been assessed. Emerging imaging and modeling techniques now allow for serial, non-invasive estimation of infarct material properties. Specifically, cine MRI assesses global LV structure and function, late-gadolinium enhancement (LGE) MRI enables visualization of infarcted tissue to quantify infarct expansion, and spatial modulation of magnetization (SPAMM) tagging provides passive wall motion assessment as a measure of tissue strain, which can all be used to evaluate infarct properties when combined with finite element (FE) models. In this work, we investigated the temporal effects of degradable hyaluronic acid (HA) hydrogels on global LV remodeling, infarct thinning and expansion, and infarct stiffness in a porcine infarct model for 12 weeks post-MI using MRI and FE modeling. Hydrogel treatment led to decreased LV volumes, improved ejection fraction, and increased wall thickness when compared to controls. FE model simulations demonstrated that hydrogel therapy increased infarct stiffness for 12 weeks post-MI. Thus, evaluation of myocardial tissue properties through MRI and FE modeling provides insight into the influence of injectable hydrogel therapies on myocardial structure and function post-MI.

[*]Corresponding Author: Department of Bioengineering, University of Pennsylvania, 240 Skirkanich Hall, 210 S. 33rd Street, Philadelphia, PA 19104, USA; Tel: 215-898-8537; Fax: 215-573-2071; burdick2@seas.upenn.edu.

Publisher's Disclaimer: This is a PDF file of an unedited manuscript that has been accepted for publication. As a service to our customers we are providing this early version of the manuscript. The manuscript will undergo copyediting, typesetting, and review of the resulting proof before it is published in its final citable form. Please note that during the production process errors may be discovered which could affect the content, and all legal disclaimers that apply to the journal pertain.

Author Manuscript Author Manuscript Author Manuscript Author Manuscript

Keywords

Hyaluronic Acid; Hydrogel; Left Ventricular Remodeling; Mechanical Properties; Magnetic Resonance Imaging; Finite Element Analysis

1. Introduction

Heart failure is a leading cause of death and disability, affecting 23 million individuals worldwide and 6 million in the U.S. [1, 2]. Nearly 70% of heart failure cases are attributed to left ventricular (LV) remodeling initiated by myocardial infarction (MI) [3]. LV remodeling is manifest by progressive LV dilation and loss of global contractile function [4]. Infarct expansion (stretching) initiates and sustains adverse left LV remodeling after MI. Immediately after the onset of ischemia, the infarct region ceases to contract and is subjected to the hemodynamic load produced by the remainder of the ventricle. This abnormal loading results in abrupt thinning and stretching of the infarct as well as increased mechanical stress in the perfused borderzone regions adjacent to the infarct [5–8]. In spite of increasing collagen content, infarcts can continue to expand for weeks after MI. This progressive expansion has been attributed to decreasing mechanical stiffness within the infarct and is associated with LV enlargement [9–11].

To limit infarct expansion, we initially tested and demonstrated the efficacy of numerous infarct wrapping techniques in large animal models of MI-induced LV remodeling [7, 12–14]. More recently, in an attempt to develop less invasive therapeutic strategies, we have focused on the use of injectable biomaterials to stiffen the infarct to reduce expansion [15–19]. While these studies have been encouraging, little *in vivo* data exists to describe the degree to which injectable materials influence infarct properties over time.

The goal of this study was to better understand the role that injectable hydrogels have on regional myocardial properties after MI using cardiac magnetic resonance imaging (MRI) and finite element (FE) modeling. Hydrogels were formed by crosslinking hyaluronic acid (HA), a linear polysaccharide found in native cardiac extracellular matrix (ECM) that plays a role in cardiac embryogenesis, scar reduction, cell migration and angiogenesis [20–23]. *In vivo* function was assessed in a porcine infarct model at 1, 4, 8, and 12 weeks post-MI to evaluate the temporal effect of injectable HA hydrogels on global LV remodeling, infarct thinning and expansion, and infarct stiffness over time. This study is the first to examine the influence of hydrogel therapies on infarct material properties using FE-model derived measures of passive myocardial stiffness based on *in vivo*, MRI-derived measures of regional myocardial strain.

2. Materials and methods

2.1. Synthesis of HeMA-HA macromer

HA (Lifecore) was modified to include a hydrolytically degradable group, hydroxyethyl methacrylate (HeMA; Figure 1A). Briefly, HeMA-HA was made by coupling HA-tetrabutyl-ammonium salt (HA-TBA) to 2-hydroxyethyl-methacryl-succinate (HeMA-COOH) using 4-dimethylamino-pyridine (DMAP, Sigma) and the coupling agent di-t-butyl

Author Manuscript Author Manuscript Author Manuscript Author Manuscript

di-carbonate (BOC_2O, Sigma) for 20 hours at 45°C (Figure S1A) [15]. The macromer was purified by dialyzing against deionized (DI) water at 4°C, acetone precipitating, and dialyzing again. The macromer was then lyophilized and the extent of HA modification with HeMA was assessed with ^{1}H-NMR (Bruker) (Figure S1B). Modification was altered by varying the ratio of BOC_2O to HeMA-COOH.

2.2. Hydrogel formation and characterization

Hydrogels were formed by crosslinking the methacrylate groups of HeMA-HA using a redox radical initiator system of ammonium persulfate (APS, 5 mM, Sigma) and N,N,N,N′, N′-tetramethylenediamine (TEMED, 5 mM, Sigma) [24]. Gel onset was quantified using an AR2000ex Rheometer (TA Instruments) by monitoring the storage (G′) and loss (G″) moduli over time at 37°C under 1% strain and a 1 Hz frequency in a cone-plate geometry (1°, 20 mm diameter). For *in vitro* characterization of mechanics and degradation, hydrogels were formed between two glass slides within a teflon mold sealed with vacuum grease. Compression testing was performed on hydrogels using a Dynamic Mechanical Analyzer (DMA) (Q800 TA Instruments) at a strain rate of 10%/min and compressive moduli were calculated from 10 to 20% strain [25]. Degradation was monitored in PBS at 37°C and mass loss was quantified using an uronic acid assay [26, 27]. Mechanics and degradation were assessed immediately after gelation (day 0) and at desired time points throughout degradation (i.e. days 1, 7, 14, 28, 56 and 84 after gelation).

2.3. In vivo evaluation in porcine infarct model

Fourteen male Yorkshire swine weighing 40–50 kg were enrolled in this study (*n=8* hydrogel treatment, *n=6* saline control). All animals received care in compliance with protocols approved by the University of Pennsylvania's Institutional Animal Care and Use Committee in accordance with the National Institutes of Health's "Guide for the Care and Use of Laboratory Animals" (NIH Publication 85–23, revised 1996). Baseline MRI scans were performed to evaluate LV volumes and regional strains 5–7 days prior to MI.

For infarct induction, pigs were anesthetized and the LV free wall exposed through a left thoracotomy. Animals were first sedated with intramuscular ketamine injections (25–30 mg/kg), intubated, and mechanically ventilated. General anesthesia was maintained on mixed isoflurane (1.5–3.0%) and oxygen, which was delivered by volume-controlled ventilation (tidal volume 10–15 mg/kg) [28]. A posterolateral infarction was induced by ligation of the left circumflex artery (LCX) and select obtuse marginal (OM) branches. In all cases, this pattern of coronary ligations produced an infarct comprising 20–25% of the left ventricle [29]. Akinesis of the infarcted myocardium was confirmed using intraoperative echocardiography. Following infarct induction, thin MRI compatible, platinum wire markers were sutured to the epicardium to outline the infarct area. These markers were tracked for quantitative assessment of infarct expansion over time (Figure 2A) [28].

Thirty minutes after infarction, animals received twenty evenly distributed 0.3 mL injections of either 0.9% normal saline (control) or HeMA-HA pre-hydrogel solution (treatment) throughout the infarct (Figure 2B). MRI scans were performed at one, four, eight, and twelve weeks after injection. Animals were sacrificed at 12 weeks and histological

Author Manuscript Author Manuscript Author Manuscript Author Manuscript

evaluation of Masson's Trichrome and H&E staining was performed. Morphometric analysis was performed to assess infarct and remote myocardial wall thickness using calipers [28].

2.4. MRI acquisition

Serial cardiac MRI was used to noninvasively assess global and regional cardiac structure and function in each animal through a series of three scans: 1) cine imaging to assess global LV morphology and function (Figure 2C), 2) late-gadolinium enhancement (LGE) imaging to assess infarct area thinning and expansion (Figure 2D), and 3) SPAMM (SPAtial Modulation of Magnetization) tagging to assess regional, diastolic myocardial strains (Figure 2E). MR images were acquired using a 3T Tim Magnetom Trio Scanner (Seimens, Inc.; Malvern, PA). General anesthesia was maintained throughout all imaging procedures, as described above. For each MRI scan, a high-fidelity pressure transducer (Millar Instruments; Houston, TX) was guided into the LV for cardiac gating; the measured pressure was later used as an input for a finite element (FE) model to assess *in vivo* myocardial stress-strain relationships.

LV volume imaging was performed using prospectively-gated 3D steady-state free precession (SSFP) cine MRI with the following imaging parameters: field of view = 300 × 244 mm^2, matrix size = 192 × 156, repetition time = 3.11 ms, echo time = 1.53 ms, bandwidth = 1184 Hz/pixel, slice thickness = 4 mm, averages = 2 [28]. Assessment of infarct location and wall thickness occurred fifteen minutes following intravenous injection of 0.1 mmol/kg gadobenatedimeglumine (MultiHance; Bracco Diagnostics, Princeton, NJ) using a 3D LGE spoiled gradient echo sequence with the following parameters: field of view = 350 × 350 mm^2, matrix size = 256 × 256, repetition time = 591.28 ms, echo time = 2.96 ms, inversion time = 200–300 ms, flip angle = 25°, averages = 2 [28]. Finally, regional LV strain was assessed using a 3D SPAMM tagged sequence with the following parameters: field of view = 260 × 260 mm^2, matrix size = 256 × 128, repetition time = 34.4 ms, tag spacing = 6 mm, bandwidth = 330 Hz/pixel, slice thickness = 2 mm, averages = 4 [28]. Separate scans were performed for systolic and diastolic strain assessment. Images were archived and stored off-line for post-processing.

2.5. MR image post-processing

2.5.1. LV volume measurement—Global LV structure and function was assessed from prospective SSFP cine MRI (Figure 2C). Raw short-axis images were sorted, cropped, and contrast-normalized in a custom MATLAB (Natick, MA) program to ensure homogenous LV coverage and image quality, respectively. Segmentation was performed throughout all cardiac phases using a semi-automated 3D active contour segmentation program (ITK-SNAP, open access/source) [30] using edge-based snakes to identify the LV blood volume. LV end-diastolic volume (EDV), end-systolic volume (ESV), and ejection fraction (EF) were calculated throughout the cardiac cycle from segmented images using inputs of in-plane and through-plane spatial resolution.

2.5.2. Infarct thickness and volume assessment—Myocardial wall thickness was measured throughout the study from cine MRI images at end diastole. Thirty radially-

Author Manuscript Author Manuscript Author Manuscript Author Manuscript

oriented spokes were randomly positioned throughout each 3D infarct area in fifteen mid-ventricular slices using ImageJ software (NIH; Bethesda, MD). Platinum markers placed immediately post-MI and LGE images were used to confirm infarct boundaries. Infarct thickness was computed at each time point from the average spoke length. Remote wall thickness was measured as a comparison.

Infarct surface area and volume were assessed at end diastole from the LGE images at each imaging time point using MIPAV software (NIH; Bethesda, MD; Figure 2D). Both infarct surface area and volume were normalized to total LV surface area and volume for each data set, respectively. The epicardium, endocardium, and infarct regions were manually contoured in fifteen slices from base to apex. The infarct was identified from the enhanced region in the LGE images and confirmed by comparing to platinum marker locations in the cine and SPAMM images. Surface area was calculated by multiplying contour perimeters by the slice thickness (4 mm) and number of analyzed slices. Volume was calculated by converting LGE image contours to binary masks to sum the voxels and computing a volume based on the spatial resolution ($1.37\times1.37\times4.00$ mm^3). It should be noted that the epicardial, endocardial, and infarct contours were the same for both the surface area and volume calculations.

2.5.3. Myocardial strain analysis—Regional wall function was assessed in terms of passive properties using diastolic strains. Regional strains were calculated from 3D SPAMM acquisitions using an optical flow technique (Figure 2E) [31]. Raw short-axis SPAMM images were first manually cropped in ImageJ to include only the LV from the apex to the mitral annulus. Epicardial and endocardial contours were manually segmented at the early diastolic reference state. Image masks were created from the segmented contours to isolate the LV myocardium. A custom optical flow mapping algorithm integrated into ImageJ was used to derive high resolution, 3D displacement flow fields and strain tensors from the SPAMM images, tracking from the early diastole to end diastole [31]. The endocardial and epicardial infarct boundaries were identified using the previously placed platinum markers and confirmed by comparison with the enhanced region in the LGE images.

2.6. In vivo diastolic material property estimation

The details of the diastolic myocardial tissue property estimation scheme, which employs a combination of MRI data, FE model simulations, and numerical optimization, have been described previously [32]. Briefly, early diastole was taken to be the reference state for the animal-specific ventricular FE models since it represents a relatively stress-free state due to minimal LV pressure. LV volume was calculated at early and end diastole using endocardial contours performed at those respective time points multiplied by the spatial resolution *(area x in-plane resolution x through-plane resolution)*. Synchronous LV pressure was recorded throughout diastole and used as a pressure boundary condition in the model.

FE models were generated by fitting the MRI-derived endocardial and epicardial contours at early diastole with 3D surfaces (Rapidform; INUS Technology, Inc., Sunnyvale, CA) and filling the myocardial space with hexahedral trilinear elements (TrueGrid; XYZ Scientific, Inc., Livermore, CA, USA) [32]. The boundary between the infarct and remote region was

Author Manuscript Author Manuscript Author Manuscript Author Manuscript

defined using 3D spline curves created from MRI-derived infarct contours projected onto the endocardial and epicardial surfaces. Myofiber angles were assigned for each hexahedral element using a custom MATLAB code and assumed to vary linearly in the transmural direction. Remote angles were fixed to be 83° at the endocardial surface and −37° at the epicardial surface with respect to the circumferential direction [19, 33, 34], whereas the infarct angles were assigned via an optimization algorithm, which will be discussed later.

The myocardial tissue properties of both the control and hydrogel-injected myocardial data were described by a nearly incompressible, transversely isotropic hyperelastic constitutive model given by:

$$W=\frac{1}{2}C(e^{Q}-1) \quad (1)$$

where

$$Q=b_f E_{11}^2+b_t(E_{22}^2+E_{33}^2+E_{23}^2+E_{32}^2)+b_{fs}(E_{12}^2+E_{21}^2+E_{13}^2+E_{31}^2) \quad (2)$$

The parameters C, b_f, b_t, b_{fs}, are constants that describe diastolic myocardial tissue properties. E_{ii} are the components of the Green–Lagrange strain tensor relative to the myofiber coordinate system (E_{11} = fiber direction, E_{22} = cross-fiber in-plane direction, E_{33} = transverse-fiber direction). The remaining E_{ij} parameters are shear strains [32]. Similar to Kichula et al. [19], the same constitutive law was used to describe both the saline- and hydrogel-treated infarcts so that differences in myocardial stiffness could be attributed to altered tissue parameters with hydrogel delivery. The strain energy function (Equation 1) was implemented using LS-DYNA (Livermore Software Technology Corporation; Livermore, CA, USA).

Subsequently, LS-OPT software (Livermore Software Technology Corporation; Livermore, CA, USA) was used to determine the optimal set of infarct material parameters (Table 1; Table S1) by minimizing the error (mean standard error, MSE) between the FE model predicted strain and the *in vivo* MRI measured strain. In addition to the diastolic strain inputs, constraints on LV cavity volume were incorporated into the MSE calculation to ensure better agreement, as described earlier. The parameters obtained from the optimization were then input into an equi-biaxial extension simulation [32] to obtain representative stress-strain curves of the infarct and remote regions for the saline and hydrogel treated animals. Using a custom MATLAB code, stress was calculated for a range of strain values to facilitate a clearer interpretation of differences in myocardial tissue properties with hydrogel treatment.

2.7. Statistical analysis

Data is presented as mean ± standard deviation (SD) or mean ± standard error of the mean (SEM), as indicated in each figure legend. Comparisons were performed using unpaired two-tailed *t* tests, where $p<0.05$ was considered statistically significant.

Author Manuscript Author Manuscript Author Manuscript Author Manuscript

3. Results

3.1. In vitro characterization of selected hydrogel formulation

A single HeMA-HA hydrogel formulation was selected for *in vivo* assessment: 25% modified HeMA-HA at 8 wt% and gelled using 5 mM APS and 5 mM TEMED. Prior to its application *in vivo*, the properties of this selected formulation were characterized *in vitro*. Gelation onset occurred at 2.1 ± 0.5 min and the crosslinking reaction reached a plateau within 20 minutes (gel completion: 15.9 ± 2.9 min) after introducing the dissolved macromer to the initiators (Figure 1B). The gel onset time dictated the timing for injection *in vivo*. In addition, hydrogels were formed with an initial compressive modulus of 147.7 ± 34.2 kPa and degraded at 11.9 ± 3.6 weeks (Figure 1C). The temporal degradation (Figure S2A) and compressive mechanical (Figure S2B) profiles illustrated that hydrogels of this formulation gradually degraded and lost their mechanics over 12 weeks, which was the intended duration of the *in vivo* study.

3.2 Histological evaluation and ex vivo infarct thickness

Histological assessment of the infarct region at the terminal time point (12 weeks) was similar (i.e. extensive collagen staining, lack of functional myocytes, etc.) in both the hydrogel treated and saline control animals (Figure 3). Hydrogel did not remain in the treatment animals at 12 weeks, which is consistent with the *in vitro* degradation results (Figure 1C; Figure S2A). Infarct wall thickness was measured *ex vivo* at 12 weeks using calipers. Hydrogel treated animals had greater *ex vivo* infarct wall thickness than controls and, as a comparison, wall thickness in the infarct region was significantly smaller ($p<0.05$) than in the remote region for both groups (Figure S3).

3.3. Global LV structure and function

Analysis of the cine MRI data revealed that the injectable HeMA-HA hydrogel system led to a trend of reduced LV end systolic volumes (ESV) and end diastolic volumes (EDV) at all time points relative to saline injected control animals (Figure 4A, B). Moreover, the LV volumes in the hydrogel treated animals were significantly smaller than the volumes of the saline control animals at 1 week post-MI (EDV, $p=0.005$; ESV, $p=0.03$). However, a trend towards progressively increasing LV volumes over time was observed in both the saline control and hydrogel treatment animals. Comparison of the saline treated volumes relative to the baseline (pre-MI) volumes (EDV, 69.4 ± 7.9 mL; ESV, 35.5 ± 5.7 mL) indicated that the majority of the ventricular expansion occurred within the first week post-MI. However, there was significant variability in the data, particularly for the saline control animals. There was also one animal that in the saline control group that showed limited progression of remodeling, potentially due to a smaller initial infarct. For the saline control group, all volumes were statistically greater ($p<0.05$) than the baseline volumes. For the hydrogel treatment group, all ESV were statistically greater than baseline, whereas the EDV were not statistically different ($p>0.05$) from baseline values except for at 8 weeks ($p=0.04$).

Ventricular function measured in terms of ejection fraction (EF) tended to be greater with hydrogel therapy than saline at all time points (Figure 4C). At 8 weeks, the average EF of the hydrogel animals was significantly different ($p<0.05$) than controls. Relative to baseline

Author Manuscript Author Manuscript Author Manuscript Author Manuscript

(51.2 ± 3.5%), EFs were statistically different in the saline group at all time points and in the hydrogel group at 1 and 4 weeks post-MI. At 8 and 12 weeks post-MI, the EF of the hydrogel animals was not significantly different ($p>0.05$) than the baseline.

3.4. In vivo infarct thickness and expansion over time

Infarct wall thickness measured *in vivo* over 12 weeks from the cine data showed increased thicknesses with hydrogel therapy when compared to controls that were statistically significant past 1 week (Figure 5). Progressive infarct wall thinning occurred in both groups over time. This trend was confirmed qualitatively in the LGE MR images, where regions of enhanced signal were localized to the infarct (Figure S4). All infarct thicknesses in both groups were significantly different from the baseline posterolateral wall thickness (9.6 ± 0.4 mm) except for the hydrogel group at 1 week post-MI (8.4 ± 0.5 mm, $p=0.07$). As a comparison, the remote wall thickness remained unchanged over the 12 week study for both groups (average over time points: hydrogel, 9.5 ± 0.1 mm; saline, 9.6 ± 0.1 mm) and there was no statistically significant difference when compared to the baseline value at each time point (baseline, 9.6 ± 0.2 mm).

Changes in infarct expansion were assessed by analyzing the LGE MR images to measure infarct surface area and infarct volume. Infarct surface areas normalized to the total LV surface area were maintained throughout the duration of the study in both the hydrogel and saline groups without statistically significant differences between the two groups (Figure S5A). Thus, the infarct surface area expanded at the same rate as the LV surface area over the course of the study. In contrast, infarct volumes normalized to the total LV volumes were maintained in the animals with hydrogel injections but decreased in saline treated animals over the four time points (Figure S5B). Beyond 1 week post-MI, the infarct volume in the hydrogel animals was significantly different ($p<0.05$) than the control animals.

3.5. Estimation of in vivo diastolic myocardial properties using FE modeling

Animal-specific FE models were used to predict diastolic strains for a given applied pressure, as a measure of passive myocardial properties (Figure 6; Figure S6). The constitutive model parameters (C, b_f, b_t, b_{fs}) and infarct fiber angles were determined via optimization to represent the unique diastolic myocardial material properties for each treatment and control animal at each time point (Table 1; Table S1). The MSE values, which describe the degree of error between the MRI-derived and FE-model predicted strains, range from 6.1 ± 1.5 to 11.3 ± 9.5. The average MSE values are consistent with previous studies [11, 35] and imply good agreement between the data and models. In addition, the values were comparable over the different time points and similar but slightly less for the hydrogel data relative to the saline control data. The optimized infarct fiber angles ranged from −33.5 ± 25.7° to −2.2 ± 3.1 ° at the epicardial surface and 9.2 ± 15.4° to 56.8 ± 16.8° at the endocardial surface. In both animal conditions, the fiber angles were closer to 0° at the epicardial than the endocardial surface, where the proximity to 0° dictates the degree of circumferential orientation of the fibers. Moreover, comparison of the fiber angles between the hydrogel and saline data sets revealed that the epicardial fiber angles were closer to 0° in the hydrogel data but the endocardial angles were closer to 0° in the saline data. Over time, the epicardial fiber angles increased to be further away from 0°, whereas the endocardial

Author Manuscript Author Manuscript Author Manuscript Author Manuscript

angles decreased closer to 0° in both conditions. Using the optimized parameters, FE models showed small strains in the infarct region that increased outward to the surrounding remote regions in both animal conditions (Figure 7). In addition, both the remote and infarct strains increased over the duration of the study.

To better understand differences in passive myocardial properties, simulated equi-biaxial tests were used to estimate stress over a given range of strain values and generate stress-strain curves in the fiber and cross-fiber directions. The range of Green–Lagrange strains investigated was determined from the FE model predicted diastolic strains (Figure 7). Examination of the stress-strain curves revealed stiffening of the infarct region in both the hydrogel and saline animals at 1 week following infarct induction when compared to baseline (Figure 8). With each subsequent time point, the infarct became progressively less stiff in both animal groups, yet remained stiffer than at baseline even out to 12 week post-MI. These trends were consistent between the fiber and cross-fiber direction but the stiffness in the fiber direction was greater than the cross-fiber direction at each time point when comparing within each animal condition. Most importantly, at each time point, the stiffness of the infarct in the hydrogel treated animals was greater than that of saline injected animals in both the fiber and cross-fiber directions.

Quantification of the moduli from the stress-strain plots over different strain ranges (0–0.05 and 0.05–0.10) further confirmed greater infarct stiffness with hydrogel therapy relative to the control animals at each time point out to 12 weeks, particularly in the fiber direction (Figure 9). In addition, infarct stiffness was greater with extension simulated in the fiber direction than in the cross-fiber direction and this stiffening response progressively declined with time. Overall, there was a persistent trend towards increased infarct stiffness in the treatment animals throughout the study but limited statistical significance between treatment and control moduli due to a relatively small sample size and inter-subject variability. For the 0–0.05 strain range, moduli were not statistically significant compared to baseline except for the hydrogel group at 12 weeks in the fiber direction ($p=0.01$) and the saline group at 8 weeks in the fiber direction ($p=0.03$) and at 4 and 8 weeks in the cross-fiber direction (4 weeks, $p=0.03$; 8 weeks, $p=0.04$). For the 0.05–0.10 strain range, moduli were not significantly significant than baseline aside from in the cross-fiber direction for the hydrogel group at 12 weeks ($p=0.03$) and the saline group at 8 weeks ($p=0.03$).

4. Discussion

It has become evident that the regional mechanical changes in the myocardium must be considered when designing biomaterial approaches for MI stabilization [4,9,36]. Previous biomaterial studies designed to alter myocardial mechanics post-MI have demonstrated that the delivery of injectable materials leads to thicker, stiffer infarcts with limited infarct expansion and preserved LV geometry [15, 16, 37–43]. However, a better understanding of the correlations between myocardial tissue properties and improved global outcomes is needed to identify optimal biomaterial properties and improve therapy design. Towards this goal, this work used MRI and FE modeling as tools to temporally examine the impact of an injectable hydrogel system on infarct tissue properties (i.e., thickness, expansion, stiffening).

Author Manuscript Author Manuscript Author Manuscript Author Manuscript

In this study, a HA hydrogel formulation with high initial mechanics was applied *in vivo* to investigate its ability to alter infarct thickness and stiffening post-MI. Previous *in vivo* work demonstrated that HA hydrogels that were present for over eight weeks with initial mechanics greater than that of the normal myocardium were more effective at maintaining LV structure post-MI than hydrogels with lower mechanics [15, 16]. Moreover, FE modeling using experimentally derived biaxial inputs from HA hydrogel-myocardial composites indicated that a formulation that is overall stiffer will further reduce wall stress to attenuate remodeling [19]. Thus, a single hydrogel formulation was selected for *in vivo* application with an *in vitro* degradation profile greater than eight weeks and an initial compressive modulus greater than ten times that of the normal myocardium. LGE MR images throughout the 12 week study correlated with the *in vitro* degradation profile (Figure 1C; Figure S2A) in that the material appeared to be present in the infarct region at the 8 week time point but was no longer present at 12 weeks (Figure S4). This was further confirmed by histology where no hydrogel was observed at the terminal time point (Figure 3). Remodeling post-MI was evaluated using MRI at 1, 4, 8, and 12 weeks following injection of either hydrogel therapy or saline for controls.

In this study, the hydrogel therapy was delivered early post-MI to reduce animal mortality by limiting the number of surgical procedures. Other groups have delivered materials at various times, ranging from immediately after MI [44] out to two months post-MI [39], where greater improvement in ventricular function was generally observed with earlier injections prior to irreversible damage. For this work, the selected timing of thirty minutes post-MI is not directl clinical relevant because the average time between the onset of MI symptoms to hospital intervention is 2–6 hours [45, 46]. Moreover, the timing of delivery in the remodeling process (i.e., acute vs. chronic) may play a role in the overall outcomes. Percutaneous delivery systems are now being developed for such HA hydrogels for future investigation.

The impact of hydrogel delivery on LV remodeling was first examined in terms of global LV structure and function. As expected, intramyocardial hydrogel injection resulted in a trend of preserved LV geometry and improved cardiac function as compared to saline delivery at all time points (Figure 4). Although both groups demonstrated signs of adverse remodeling relative to baseline, the ability of hydrogel therapy to minimize LV dilation was maintained over the 12 week study. These findings correlated with our previous echocardiographic studies that demonstrated better maintenance of LV structure with HA hydrogel injection compared to infarct controls in an ovine infarct model [15, 16]. To expand upon our previous work, the current study used state-of-the-art MRI to serially examine the impact of hydrogels on *in vivo* infarct thinning and expansion and passive myocardial stiffening to better understand how hydrogel therapy led to these positive global outcomes.

Thinning of the myocardium post-MI has been identified as an important contributor to increased wall stress, both in the infarct and surrounding borderzone regions. Thus, myocardial thickness was measured to assess the ability of hydrogel therapy to bulk and stabilize the heart wall to attenuate remodeling. As anticipated, *ex vivo* assessment at 12 weeks (Figure S3) and *in vivo* assessment over the 12 weeks demonstrated increased infarct

Author Manuscript Author Manuscript Author Manuscript Author Manuscript

thickness due to hydrogel bulking (Figure 5). Many studies have demonstrated similar increases in *ex vivo* infarct thickness with material delivery [15, 16, 43], but few have quantified infarct thinning noninvasively over time, as in this study [28].

The infarct expansion that occurs as the heart dilates and myocardial walls thin both precipitates and sustains remodeling [6, 47–49]. Thus, the impact of hydrogel injection on infarct expansion (i.e., stretching) was assessed by measuring the infarct surface area and volume and normalizing to total LV surface area and volume, respectively. Infarct surface area is primarily a measure of infarct expansion, whereas infarct volume accounts for both thinning and expansion. The minimal change in infarct surface area over time and between groups (Figure S5A) suggests that the rate of infarct expansion was similar to the rate of global LV dilation (Figure 4A, B). However, since there was less overall LV dilation with hydrogel therapy at each time point, the infarct in the hydrogel treated animals expanded less than in controls. Moreover, the maintained infarct volume over the four time points with hydrogel therapy (Figure S5B) correlates with the minimal changes in infarct thickness (Figure 5C, D) and infarct surface area as a measure of expansion (Figure S5A). Similarly, the decrease in infarct volume over time in controls correlates with the thinning observed due to matrix degradation in the infarct (Figure 5) [50] since minimal changes were observed in the rate of infarct expansion (Figure S5B). Thus, infarct surface area assessment showed less infarct expansion with hydrogel therapy due to less LV dilation, whereas infarct volume assessment further confirmed the trends in infarct thickness in that hydrogels function by bulking the myocardial wall.

Due to the role of increased infarct compliance in sustaining adverse remodeling [51, 52], MRI-derived diastolic strains were input into a FE model to directly quantify *in vivo* passive mechanical properties in the myocardium and provide an understanding of the impact of hydrogel delivery on *in vivo* wall compliance (Figure 6; Figure S6). Assessment of regional stress-strain relationships using simulated equi-biaxial extension tests demonstrated that hydrogel injection led to increased myocardial stiffness in the infarct region relative to controls, with a larger impact on mechanics in the fiber direction as compared to the cross-fiber direction (Figure 8; Figure 9). In both animal groups, extensive stiffening of the infarct was observed at 1 week post-MI compared to baseline and the stiffening response progressively decreased over time. Immediately post-MI, the infarct loses its systolic, contractile function whereas diastolic function is relatively maintained. This abrupt transition from an active to passive material leads to immediate stretching and thinning of the infarct, as well as LV dilation [36, 53, 54]. The initial stiffening response viewed over the first week relative to baseline (Figure 8; Figure 9) can thus be attributed to the interstitial edema and infiltration of inflammatory cells in the early post-MI necrotic period [9, 36], which only temporarily limit the outward expansion of the infarct. Despite the increase in collagen content as the infarct heals with time, there is a gradual decrease in infarct stiffness (Figure 8; Figure 9) as infarct expansion (Figure S5) and global LV dilation progress (Figure 4). The increased stiffening with hydrogel injection indicates that the hydrogel successfully altered the material properties of the infarct prior to when the body had compensated for remodeling, leading to less infarct expansion and LV dilation.

Author Manuscript Author Manuscript Author Manuscript Author Manuscript

The increased infarct stiffness (Figure 9) and thickness (Figure 5) with HeMA-HA injection is likely due to a combination of the presence of the hydrogel itself, as well as a biological response to the material injection [55]. From the *in vitro* hydrogel characterization (Figure 1C; Figure S2), the selected hydrogel formulation degrades prior to 12 weeks; yet, the infarct wall thickness at 12 weeks is greater in the hydrogel treated animals when compared to the saline injected animals, despite material degradation (Figure 5). This maintained thickness suggests a response to the HA hydrogel, which could include the degradation products of HA due to its native functions or an inflammatory response that leads to collagen production [20–23]. We have previously characterized the tissue response to injected HeMA-HA hydrogels delivered to the myocardium and observed positive MHC Class II staining at the biomaterial interface indicative of an inflammatory response and positive α-smooth muscle actin (α-SMA) staining in sections of the infarct region indicative of neovascularization [15]. There are no cytotoxicity concerns with the hydrogel degradation products or the chemical initiators used for crosslinking based on previous *in vitro* biocompatibility assessments by our group [16].

Overall, the use of MRI and FE modeling to serially assess key infarct parameters (i.e., thickening, expansion, stiffening) demonstrated that the infarcts of control animals progressively thinned over the 12 week study (Figure 5) and became less stiff, particularly in the fiber direction out to 8 weeks, at which point the infarct stiffness stabilized out to 12 weeks (Figure 8; Figure 9). Whereas the greatest global ventricular changes in the control animals were observed from pre-MI to one week post-MI (Figure 4), regional myocardial assessment demonstrated a progressive decline in infarct properties throughout the 12 weeks (Figure 5; Figure 9; Figure S5). In contrast to saline delivery, HA hydrogel delivery not only limited global dilation (Figure 4) but also thickened (Figure 5) and stiffened the infarct in the fiber direction throughout the study (Figure 8; Figure 9). While the benefit of hydrogel therapy on global LV remodeling was maintained over the 12 weeks (Figure 4), both infarct thickness and stiffness progressively decreased as the material degraded (Figure S2). The gradual decrease in infarct modulus with hydrogel therapy (Figure 9) tracks with the decrease in hydrogel mechanics over time (Figure S2), highlighting that the material itself plays a dominant role in infarct stiffening. Moreover, the technique of combining MRI-derived measures of strain with FE model-generated stresses can not only assess infarct specific properties but simultaneously document the decrease in mechanical properties of the hydrogel. Thus, future work should focus on biomaterials that maintain their mechanics for longer durations or those that alter the biology of the healing infarct.

5. Conclusions

An injectable, degradable hydrogel was successfully applied to an *in vivo* porcine infarct model to serially examine its effect on the physical properties of the infarct region using MRI and FE modeling. MRI analysis demonstrated that injectable HA hydrogels can improve LV structure and function, preserve infarct thickness, and limit infarct dilation. Building upon our previous work, input of MRI-derived diastolic strain parameters into a FE model indicated that the hydrogel delivery increased infarct stiffness throughout the 12 week study when compared to saline-treated controls. In summary, evaluation of myocardial properties using MRI and FE modeling improves our understanding of the impact of

Author Manuscript Author Manuscript Author Manuscript Author Manuscript

injectable materials on the post-MI remodeling process and can serve as a tool to determine the optimal biomaterial properties for MI stabilization.

Supplementary Material

Refer to Web version on PubMed Central for supplementary material.

Acknowledgments

The authors would like to acknowledge financial support from the National Institutes of Health (T32 HL007954, R01 HL73021, R01 HL063954, R01 HL111090) and the American Heart Association (14BGIA18850020 to JFW, Established Investigator Award to JAB).

References

1. Bui AL, Horwich TB, Fonarow GC. Epidemiology and risk profile of heart failure. Nat Rev Cardiol. 2011; 8:30–41. [PubMed: 21060326]
2. Go AS, Mozaffarian D, Roger VL, Benjamin EJ, Berry JD, Blaha MJ, et al. Heart disease and stroke statistics-2014 update: A report from the American Heart Association. Circulation. 2014; 129:e28–e292. [PubMed: 24352519]
3. Gheorghiade M, Bonow RO. Chronic heart failure in the United States: A manifestation of coronary artery disease. Circulation. 1998; 97:282–9. [PubMed: 9462531]
4. Buckberg GD. Architecture must document functional evidence to explain the living rhythm. Eur J Cardiothorac Surg. 2005; 27:202–9. [PubMed: 15691671]
5. Jackson BM, Gorman JH 3rd, Salgo IS, Moainie SL, Plappert T, St John-Sutton M, et al. Border zone geometry increases wall stress after myocardial infarction: Contrast echocardiographic assessment. Am J Physiol Heart Circ Physiol. 2003; 284:H475–9. [PubMed: 12414441]
6. Kramer CM, Lima JA, Reichek N, Ferrari VA, Llaneras MR, Palmon LC, et al. Regional differences in function within noninfarcted myocardium during left ventricular remodeling. Circulation. 1993; 88:1279–88. [PubMed: 8353890]
7. Pilla JJ, Blom AS, Gorman JH 3rd, Brockman DJ, Affuso J, Parish LM, et al. Early postinfarction ventricular restraint improves borderzone wall thickening dynamics during remodeling. Ann Thorac Surg. 2005; 80:2257–62. [PubMed: 16305885]
8. Epstein FH, Yang Z, Gilson WD, Berr SS, Kramer CM, French BA. MR tagging early after myocardial infarction in mice demonstrates contractile dysfunction in adjacent and remote regions. Magn Reson Med. 2002; 48:399–403. [PubMed: 12210951]
9. Gupta KB, Ratcliffe MB, Fallert MA, Edmunds LH Jr, Bogen DK. Changes in passive mechanical stiffness of myocardial tissue with aneurysm formation. Circulation. 1994; 89:2315–26. [PubMed: 8181158]
10. Wenk JF, Klepach D, Lee LC, Zhang Z, Ge L, Tseng EE, et al. First evidence of depressed contractility in the border zone of a human myocardial infarction. Ann Thorac Surg. 2012; 93:1188–94. [PubMed: 22326127]
11. Wenk JF, Sun K, Zhang Z, Soleimani M, Ge L, Saloner D, et al. Regional left ventricular myocardial contractility and stress in a finite element model of posterobasal myocardial infarction. J Biomech Eng -Trans ASME. 2011; 133:044501.
12. Pilla JJ, Blom AS, Brockman DJ, Bowen F, Yuan Q, Giammarco J, et al. Ventricular constraint using the acorn cardiac support device reduces myocardial akinetic area in an ovine model of acute infarction. Circulation. 2002; 106:I207–11. [PubMed: 12354735]
13. Pilla J, Blom A, Brockman D, Ferrari V, Yuan D, Acker M. Passive ventricular constraint to improve left ventricular function and mechanics in an ovine model of heart failure secondary to acute myocardial infarction. J Thorac Cardiovasc Surg. 2003; 126:1467–76. [PubMed: 14666021]
14. Kelley ST, Malekan R, Gorman JH 3rd, Jackson BM, Gorman RC, Suzuki Y, et al. Restraining infarct expansion preserves left ventricular geometry and function after acute anteroapical infarction. Circulation. 1999; 99:135–42. [PubMed: 9884390]

Author Manuscript Author Manuscript Author Manuscript Author Manuscript

15. Tous E, Ifkovits JL, Koomalsingh KJ, Shuto T, Soeda T, Kondo N, et al. Influence of injectable hyaluronic acid hydrogel degradation behavior on infarction-induced ventricular remodeling. Biomacromolecules. 2011; 12:4127–35. [PubMed: 21967486]
16. Ifkovits JL, Tous E, Minakawa M, Morita M, Robb JD, Koomalsingh KJ, et al. Injectable hydrogel properties influence infarct expansion and extent of postinfarction left ventricular remodeling in an ovine model. Proc Natl Acad Sci U S A. 2010; 107:11507–12. [PubMed: 20534527]
17. Wenk JF, Wall ST, Peterson RC, Helgerson SL, Sabbah HN, Burger M, et al. A method for automatically optimizing medical devices for treating heart failure: Designing polymeric injection patterns. J Biomech Eng. 2009; 131:121011-1–7. [PubMed: 20524734]
18. Wenk JF, Eslami P, Zhang Z, Xu C, Kuhl E, Gorman, Joseph H III, et al. A novel method for quantifying the in-vivo mechanical effect of material injected into a myocardial infarction. Ann Thorac Surg. 2011; 92:935–41. [PubMed: 21871280]
19. Kichula ET, Wang H, Dorsey SM, Szczesny SE, Elliott DM, Burdick JA, et al. Experimental and computational investigation of altered mechanical properties in myocardium after hydrogel injection. Ann Biomed Eng. 2014; 42:1546–56. [PubMed: 24271262]
20. Burdick JA, Prestwich GD. Hyaluronic acid hydrogels for biomedical applications. Adv Mater. 2011; 23:H41–56. [PubMed: 21394792]
21. Li Y, Toole BP, Dealy CN, Kosher RA. Hyaluronan in limb morphogenesis. Dev Biol. 2007; 305:411–20. [PubMed: 17362908]
22. Toole BP. Hyaluronan: From extracellular glue to pericellular cue. Nat Rev Cancer. 2004; 4:528–39. [PubMed: 15229478]
23. Toole BP. Hyaluronan in morphogenesis. J Intern Med. 1997; 242:35–40. [PubMed: 9260564]
24. Temenoff, JS.; Kasper, FK.; Mikos, AG. Fumarate-based macromers as scaffolds for tissue engineering applications. In: Ashammakhi, N.; Reis, R.; Chiellini, E., editors. Topics in Tissue Engineering. 3. Oulu, Finland: University of Oulu; 2007. p. 6.1-6.16.
25. Anseth KS, Bowman CN, Brannon-Peppas L. Mechanical properties of hydrogels and their experimental determination. Biomaterials. 1996; 17:1647–57. [PubMed: 8866026]
26. Bitter T, Muir HM. A modified uronic acid carbazole reaction. Anal Biochem. 1962; 4:330–4. [PubMed: 13971270]
27. Platzer M, Ozegowski JH, Neubert RH. Quantification of hyaluronan in pharmaceutical formulations using high performance capillary electrophoresis and the modified uronic acid carbazole reaction. J Pharm Biomed Anal. 1999; 21:491–6. [PubMed: 10701415]
28. McGarvey, JM.; Kondo, N.; Witschey, WRT.; Takebe, M.; Aoki, C.; Burdick, JA., et al. Injectable microsphere gel progressively improves global ventricular function, regional contractile strain, and mitral regurgitation after myocardial infarction. in review
29. Witschey WRT, Pilla JJ, Ferrari G, Koomalsingh K, Haris M, Hinmon R, et al. Rotating frame spin lattice relaxation in a swine model of chronic, left ventricular myocardial infarction. Magn Reson Med. 2010; 64:1454–61.
30. Yushkevich PA, Piven J, Hazlett HC, Smith RG, Ho S, Gee JC, et al. User-guided 3D active contour segmentation of anatomical structures: Significantly improved efficiency and reliability. Neuroimage. 2006; 31:1116–28. [PubMed: 16545965]
31. Xu C, Pilla JJ, Isaac G, Gorman JH 3rd, Blom AS, Gorman RC, et al. Deformation analysis of 3D tagged cardiac images using an optical flow method. J Cardiovasc Magn Reson. 2010; 12:19. [PubMed: 20353600]
32. Mojsejenko D, McGarvey JR, Dorsey SM, Gorman JH 3rd, Burdick JA, Pilla JJ, et al. Estimating passive mechanical properties in a myocardial infarction using MRI and finite element simulations. Biomech Model Mechanobiol. 2014
33. Lee W, Pernot M, Couade M, Messas E, Bruneval P, Bel A, et al. Mapping myocardial fiber orientation using echocardiography-based shear wave imaging. IEEE Trans Med Imaging. 2012; 31:554–62. [PubMed: 22020673]
34. Hooks DA, Trew ML, Caldwell BJ, Sands GB, LeGrice IJ, Smaill BH. Laminar arrangement of ventricular myocytes influences electrical behavior of the heart. Circ Res. 2007; 101:E103–12. [PubMed: 17947797]

Author Manuscript Author Manuscript Author Manuscript Author Manuscript

35. Sun K, Stander N, Jhun C, Zhang Z, Suzuki T, Wang G, et al. A computationally efficient formal optimization of regional myocardial contractility in a sheep with left ventricular aneurysm. J Biomech Eng -Trans ASME. 2009; 131:111001.
36. Holmes JW, Borg TK, Covell JW. Structure and mechanics of healing myocardial infarcts. Annu Rev Biomed Eng. 2005; 7:223–53. [PubMed: 16004571]
37. Morita M, Eckert CE, Matsuzaki K, Noma M, Ryan LP, Burdick JA, et al. Modification of infarct material properties limits adverse ventricular remodeling. Ann Thorac Surg. 2011; 92:617–25. [PubMed: 21801916]
38. Ryan LP, Matsuzaki K, Noma M, Jackson BM, Eperjesi TJ, Plappert TJ, et al. Dermal filler injection: A novel approach for limiting infarct expansion. Ann Thorac Surg. 2009; 87:148–55. [PubMed: 19101288]
39. Landa N, Miller L, Feinberg MS, Holbova R, Shachar M, Freeman I, et al. Effect of injectable alginate implant on cardiac remodeling and function after recent and old infarcts in rat. Circulation. 2008; 117:1388–96. [PubMed: 18316487]
40. Mukherjee R, Zavadzkas JA, Saunders SM, McLean JE, Jeffords LB, Beck C, et al. Targeted myocardial microinjections of a biocomposite material reduces infarct expansion in pigs. Ann Thorac Surg. 2008; 86:1268–76. [PubMed: 18805174]
41. Dobner S, Bezuidenhout D, Govender P, Zilla P, Davies N. A synthetic non-degradable polyethylene glycol hydrogel retards adverse post-infarct left ventricular remodeling. J Card Fail. 2009; 15:629–36. [PubMed: 19700140]
42. Rane AA, Christman KL. Biomaterials for the treatment of myocardial infarction: A 5-year update. J Am Coll Cardiol. 2011; 58:2615–29. [PubMed: 22152947]
43. Dorsey, SM.; Burdick, JA. Hydrogels for cardiac repair. In: Khademhosseini, A.; Demirci, U., editors. Applications of Hydrogels in Regenerative Medicine. in press
44. Kofidis T, Lebel DR, Martinez EC, Hoyt G, Tanaka M, Robbins RC. Novel injectable bioartificial tissue facilitates targeted, less invasive, large-scale tissue restoration on the beating heart after myocardial injury. Circulation. 2005; 112:I173–7. [PubMed: 16159811]
45. Jneid H, Fonarow GC, Cannon CP, Palacios IF, Kilic T, Moukarbel GV, et al. Impact of time of presentation on the care and outcomes of acute myocardial infarction. Circulation. 2008; 117:2502–9. [PubMed: 18427127]
46. Miura T, Miki T. Limitation of myocardial infarct size in the clinical setting: Current status and challenges in translating animal experiments into clinical therapy. Basic Res Cardiol. 2008; 103:501–13. [PubMed: 18716709]
47. Jackson BM, Gorman JH 3rd, Moainie SL, Guy TS, Narula N, Narula J, et al. Extension of borderzone myocardium in postinfarction dilated cardiomyopathy. J Am Coll Cardiol. 2002; 40:1160, 7. discussion 1168–71. [PubMed: 12354444]
48. Weisman HF, Healy B. Myocardial infarct expansion, infarct extension, and reinfarction - Pathophysiologic concepts. Prog Cardiovasc Dis. 1987; 30:73–110. [PubMed: 2888158]
49. Erlebacher JA, Weiss JL, Weisfeldt ML, Bulkley BH. Early dilation of the infarcted segment in acute transmural myocardial-infarction - Role of infarct expansion in acute left-ventricular enlargement. J Am Coll Cardiol. 1984; 4:201–8. [PubMed: 6234343]
50. Mukherjee R, Brinsa TA, Dowdy KB, Scott AA, Baskin JM, Deschamps AM, et al. Myocardial infarct expansion and matrix metalloproteinase inhibition. Circulation. 2003; 107:618–25. [PubMed: 12566376]
51. Pilla JJ, Gorman JH 3rd, Gorman RC. Theoretic impact of infarct compliance on left ventricular function. Ann Thorac Surg. 2009; 87:803–11. [PubMed: 19231393]
52. Pilla, JJ.; Koomalsingh, KJ.; McGarvey, JM.; Witschey, WRT.; Dougherty, L.; Gorman, JH., 3rd, et al. Regional myocardial three-dimensional principal strains during post-infarction left ventricular remodeling. in review
53. Holmes JW, Nunez JA, Covell JW. Functional implications of myocardial scar structure. American Journal of Physiology-Heart and Circulatory Physiology. 1997; 272:H2123–30.
54. Guccione J, Costa K, McCulloch A. Finite-element stress-analysis of left-ventricular mechanics in the beating dog Heart. J Biomech. 1995; 28:1167–77. [PubMed: 8550635]

Author Manuscript Author Manuscript Author Manuscript Author Manuscript

55. Anderson JM, Rodriguez A, Chang DT. Foreign body reaction to biomaterials. Semin Immunol. 2008; 20:86–100. [PubMed: 18162407]

Author Manuscript Author Manuscript Author Manuscript Author Manuscript

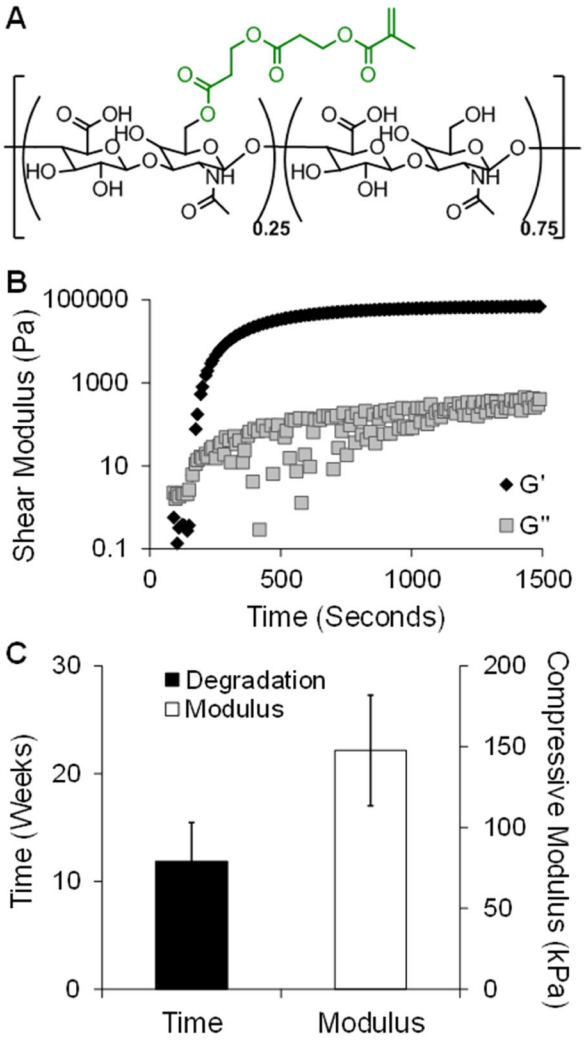

Fig. 1.

Hydrogel formation and *in vitro* characterization. Chemical structure of HeMA-HA macromer, where 25% of the HA repeat units were modified with HeMA groups (A). Representative rheological time sweep after mixing HeMA-HA macromer with APS and TEMED, where the intersection of the storage (Gprime;) and loss (G″) moduli is defined as gel onset (B). Time to complete degradation and initial mechanics of the HeMA-HA formulation used for *in vivo* studies, *n=4* (C). Data presented as mean ± SD.

Author Manuscript Author Manuscript Author Manuscript Author Manuscript

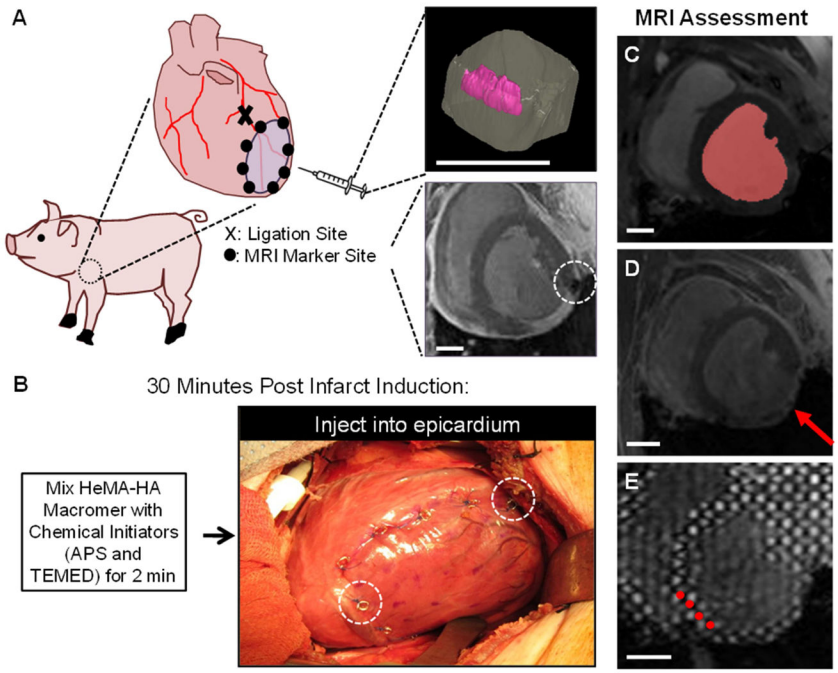

Fig. 2.

MRI analysis of *in vivo* porcine infarct model. *In vivo* function (*n=3–6/group*) was assessed in an established porcine posterior infarct model (A). Inserts in panel A show a three-dimensional MRI reconstruction of a hydrogel injection in a myocardial explant (top) and visibility of a MRI compatible marker (white, dashed circle) placed post-MI for tracking infarct expansion over time (bottom). Thirty minutes post-MI, animals underwent an array of twenty 0.3 mL injections of either prepolymer solution or saline in the infarct (B). MRI compatible markers (white, dashed circles) are visible. MRI scans were performed at baseline (i.e. prior to infarction) and at 1, 4, 8 and 12 weeks post-MI. MRI data was analyzed to assess global LV structure and function from segmentation of the blood volume (red shape) in cine MRI (C), infarct (red arrow) expansion from LGE MRI (D), and myocardial wall function from tracking grid displacement (red circles highlight select tags) in SPAMM tagged MRI (E). Scale bar = 2 cm.

Author Manuscript Author Manuscript Author Manuscript Author Manuscript

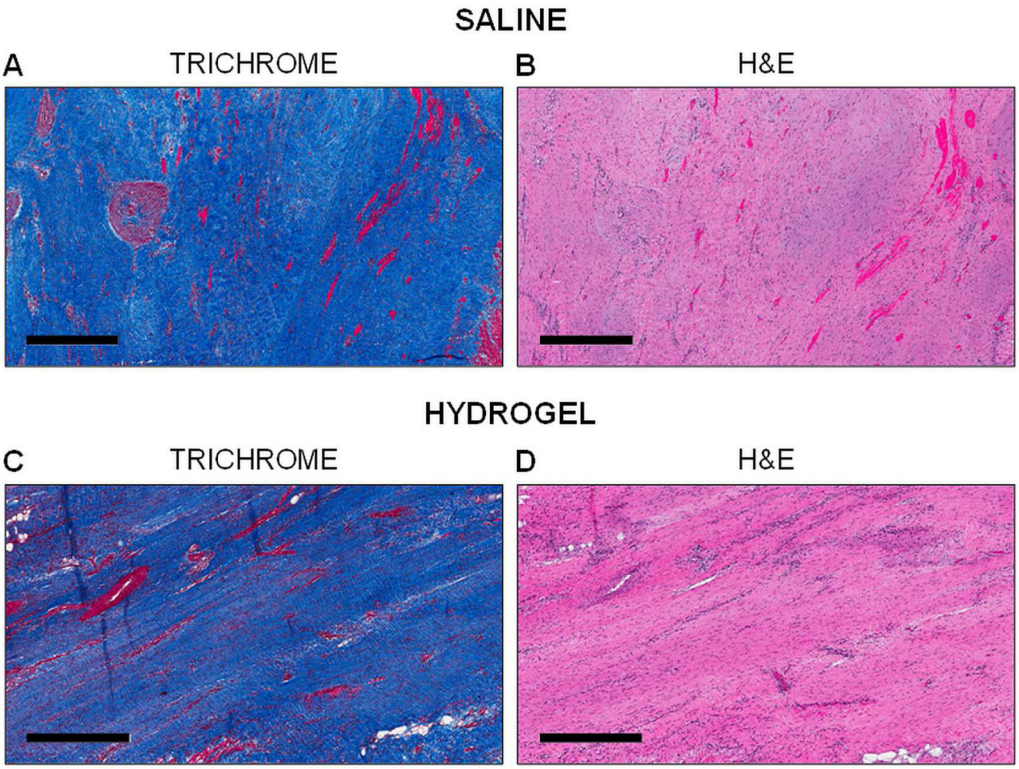

Fig. 3.

Histological assessment of infarcts. Histological evaluation using Masson's Trichrome (A, C) and H&E (B, D) stains of saline treated (A, B) and hydrogel treated (C, D) animals at 12 weeks post-MI. Scale bar = 500 μm.

Author Manuscript Author Manuscript Author Manuscript Author Manuscript

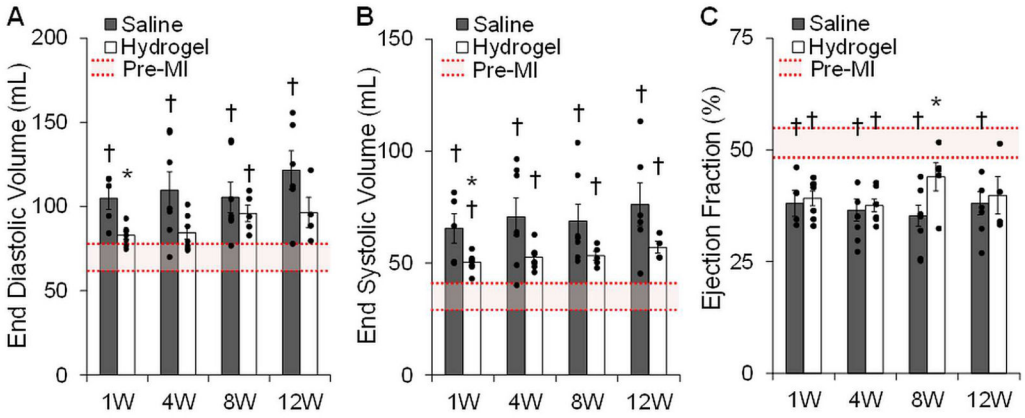

Fig. 4.

Global cardiac structural and functional outcomes. LV volume and function assessed by segmenting cine MRI images throughout all cardiac phases, *n=3–6/group*. Hydrogel treatment led to decreased LV volumes (A, B) and improved cardiac function in terms of ejection fraction (C). Data presented as mean ± SEM. **p<0.05* vs. saline controls. †*p<0.05* vs. baseline.

Author Manuscript Author Manuscript Author Manuscript Author Manuscript

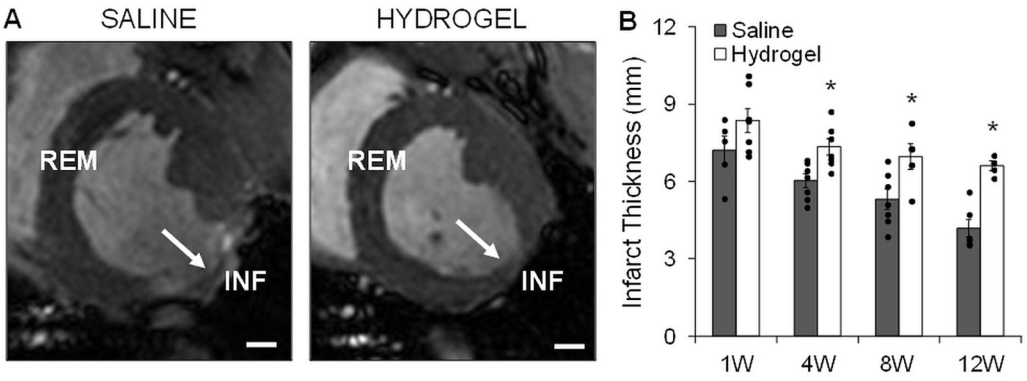

Fig. 5.

Infarct wall thicknesses measured *in vivo*. Myocardial wall thickness was measured at different locations (INF: infarct; REM: remote) *in vivo* throughout the study by analyzing cine MR images at end diastole. Representative images at 12 weeks indicating infarct region (white arrows) are shown for saline and hydrogel treated animals (A). Quantification showed increased infarct wall thickness at all time points with hydrogel therapy, *n=3–6/group* (B). Data presented as mean ± SEM. *$p<0.05$ vs. saline controls. Scale bars = 1 cm.

Author Manuscript Author Manuscript Author Manuscript Author Manuscript

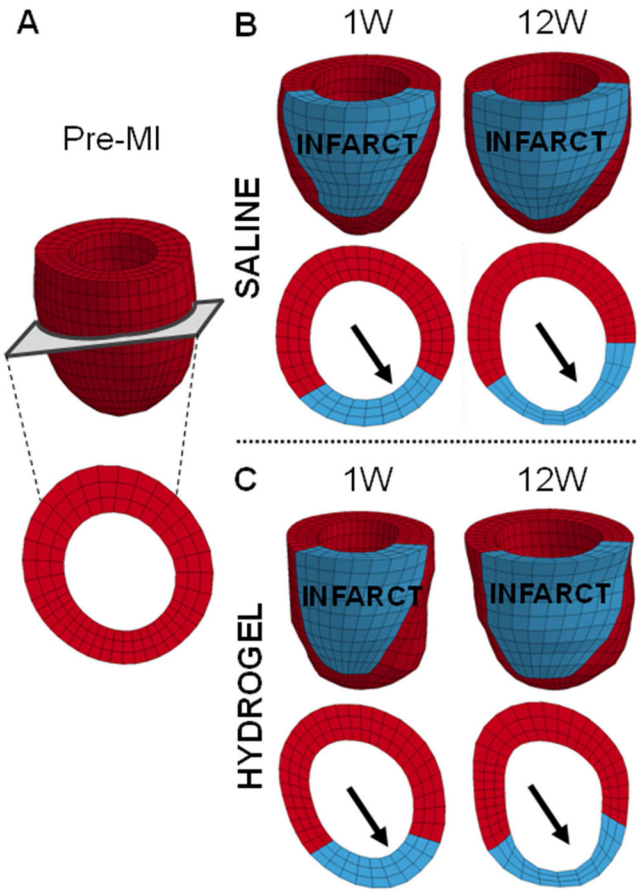

Fig. 6.

Finite element model to assess passive myocardial properties. Representative finite element models of a baseline animal (A) and saline (B) and hydrogel (C) treated animals at 1 and 12 weeks post-MI. The infarct (red) and remote (blue) regions were assigned different myocardial tissue properties. Short axis views taken from roughly the same position at mid-ventricle demonstrate thinning of the infarct region over time (arrows).

Author Manuscript Author Manuscript Author Manuscript Author Manuscript

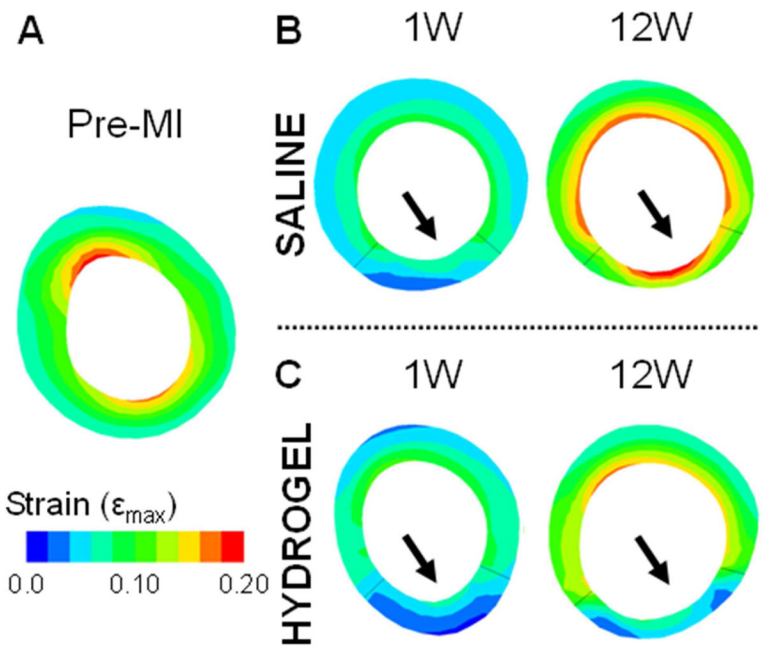

Fig. 7.

Short-axis view of the diastolic principal strain generated from FE model simulations. Representative short-axis strain maps of a baseline animal (A) and saline (B) and hydrogel (C) treated animals at 1 and 12 weeks. The end-diastolic pressure was set at a constant 10 mmHg to ensure all data sets experienced the same load.

Author Manuscript Author Manuscript Author Manuscript Author Manuscript

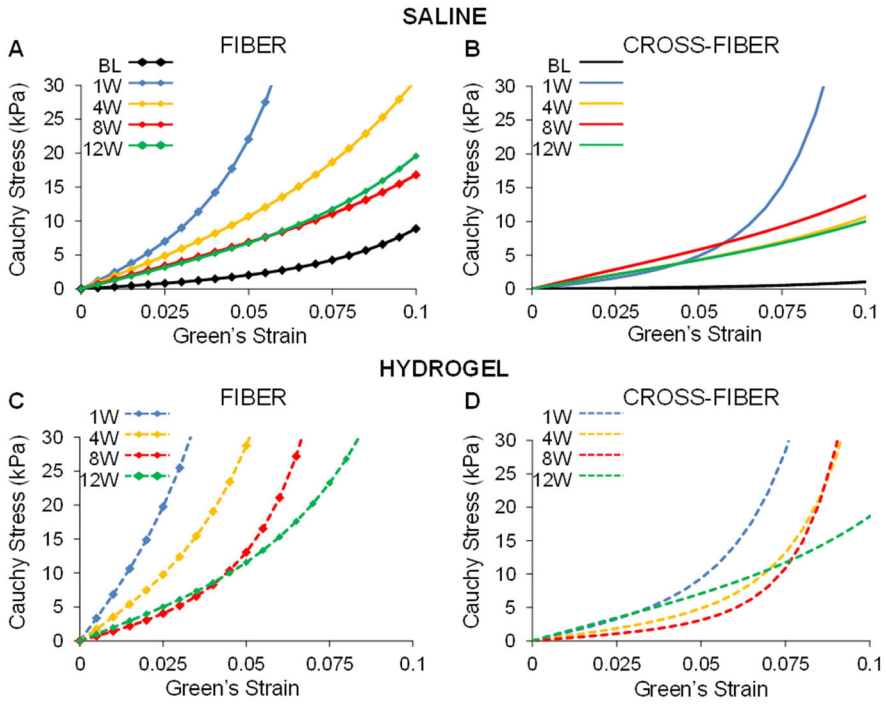

Fig. 8.

Simulated equi-biaxial extension tests using FE model optimization parameters. Stress-strain equations were implemented into a custom MATLAB code to calculate stress at the same set of strain points for each case. Average stress-strain plots of the infarct region of saline control (top) and hydrogel treated (bottom) animals in the fiber (A, C) and cross-fiber (B, D) direction in saline treated animals over time.

Author Manuscript Author Manuscript Author Manuscript Author Manuscript

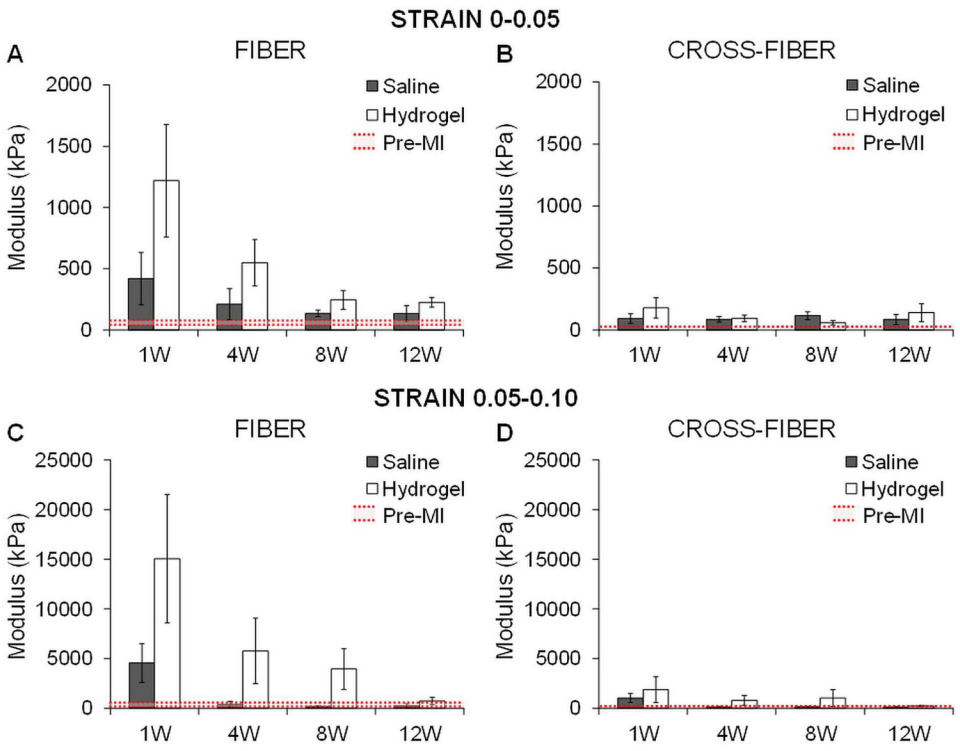

Fig. 9.

Quantification of moduli in the infarct region from simulated equi-biaxial tests. The moduli were calculated at different strain ranges for extension in both the fiber (A, C) and cross-fiber (B, D) direction in saline and hydrogel treated animals over time. Data presented as mean ± SEM.

Author Manuscript Author Manuscript Author Manuscript Author Manuscript

Table 1

Optimization results for infarct region.

		Time Point				
		Pre-MI	**1 Week**	**4 Week**	**8 Week**	**12 Week**
Saline	**C (kPa)**	0.39 ± 0.10	1.48 ± 1.40	6.08 ± 4.03	9.38 ± 5.10	4.01 ± 2.34
	b_f	72.03 ± 29.63	171.53 ± 39.78	13.77 ± 12.54	15.28 ± 19.71	19.01 ± 31.15
	b_t	5.08 ± 4.53	24.22 ± 19.62	6.58 ± 5.96	8.32 ± 4.59	8.07 ± 5.64
	b_{fs}	36.69 ± 18.23	22.25 ± 17.55	8.64 ± 2.51	25.27 ± 27.41	17.19 ± 18.13
	epi-angle (deg)		−14.89 ± 21.30	−23.00 ± 25.01	−18.15 ±21.81	−33.54 ± 25.73
	endo-angle (deg)		43.56 ± 2.50	35.66 ± 21.41	26.69 ± 14.61	9.18 ± 15.42
	MSE	8.64 ± 1.53	7.43 ± 4.02	7.62 ± 2.08	11.31 ± 9.46	8.14 ± 3.63
Hydrogel	**C (kPa)**		4.05 ± 2.86	4.38 ± 5.00	1.47 ± 1.54	5.36 ± 6.28
	b_f		137.67 ± 102.75	122.59 ± 94.49	139.26 ± 99.94	41.27 ± 67.66
	b_t		11.38 ± 6.95	9.21 ± 6.31	18.55 ± 23.25	14.46 ± 14.47
	b_{fs}		25.63 ± 21.05	30.02 ± 25.12	25.74 ± 20.63	23.54 ± 29.29
	epi-angle (deg)		−8.88 ± 15.60	−10.07 ± 17.17	−2.16 ± 3.07	−24.28 ± 20.95
	endo-angle (deg)		56.84 ± 16.75	32.07 ± 18.96	25.63 ± 17.16	28.83 ± 24.93
	MSE		6.14 ± 1.53	7.08 ± 2.16	9.81 ± 4.25	8.87 ± 3.55